Electronic properties and STM images of doped bilayer graphene

Stéphane-Olivier Guillaume,[1] Bing Zheng,[2,*] Jean-Christophe Charlier,[2] and Luc Henrard[1]
[1]*Physics Department (PMR), University of Namur (FUNDP), B-5000 Namur, Belgium*
[2]*Université catholique de Louvain (UCL), Institute of Condensed Matter and Nanosciences (IMCN), B-1348 Louvain-la-Neuve, Belgium*
(Received 31 October 2011; revised manuscript received 15 December 2011; published 27 January 2012)

Electronic structures and scanning tunneling microscopy (STM) patterns of boron- and nitrogen-doped bilayer graphene are predicted using state-of-the-art first-principles calculations. Asymmetric doping is considered, leading to different charge-carrier densities on each graphene layer and to a band-gap opening. When lying on the top layer, the local STM patterns of the dopant are predicted to be similar to images observed in monolayer graphene. In contrast, the local electronic states of the buried dopant are not directly detectable by STM. However, by analyzing the charge transfer between graphene layers and its effect on the contrast of the STM image, the chemical doping is found to affect the symmetry (hexagonal and triangular) of the observed lattice for both the top doped surface and the buried doped layer. Consequently, our *ab initio* simulations predict a possible indirect detection of *N* or *B* dopants buried in bilayer graphene when such a contrast is revealed by a series of STM images or using scanning tunneling spectroscopy.

DOI: 10.1103/PhysRevB.85.035444 PACS number(s): 73.22.Pr, 71.15.Mb, 73.20.At

I. INTRODUCTION

Multilayer graphene (MLG) presents electronic and transport properties drastically different from those of single-layer graphene (SLG). A two-dimensional monatomic sheet exhibits a linear dispersion of electronic states near the Fermi level (the massless Dirac fermions characteristic), resulting in an anomalous quantum Hall effect (QHE) and extraordinarily high electronic mobilities for the charge carries. Combined with its mechanical properties (resistance and flexibility) and its reduced light absorption, graphene-based materials have been proposed for several nanoelectronics applications, including new transparent conductive devices.[1,2] However, these remarkable electronic properties are modified by the presence of another surrounding carbon layer or a substrate. Indeed, the linear electronic dispersion disappears in the case of stacking as in MLG (except if layers are disoriented)[3–6] or when deposited on a substrate, thus inducing a strong decrease of the charge mobilities and a modification of the QHE.[7] Finally, when an external field is applied, the interaction between layers can be controlled and tailored, opening new possibilities for the engineering of the band gap in few-layer graphene.[8,9]

Chemical doping of graphene-based materials represents another research direction to tune their electronic properties in the same way as for conventional doping in semiconductor (Si, etc.). Several attempts have been reported in the literature for doping either flat graphene or carbon nanotubes (CNT's), mostly with boron (B) and nitrogen (N).[10–13] Their respective influence on the electronic and transport properties and transport have been extensively studied.[13–16] This chemical doping also induces changes in the reactivity of carbon nanostructures, thus allowing for the development of a chemical sensor[17] and the storage of energy (Li battering[18] and supercapacitor[19]).

The combined influence of both interlayer interaction and chemical doping has not been investigated in detail yet in order to interpret experimental data. To the best of our knowledge, only the effect of N, B, and K doping on the electronic structure of *AB*-stacked bilayer graphene (BLG) has been studied so far.[20] In the present study, both nitrogen and boron substitutional doping in one of the two layers of a bilayer graphene are investigated using a first-principles approach. A detailed study is performed of the scanning tunneling microscopy (STM) features for N or B chemical doping on the top layer of bilayer graphene or for a buried defect. Our simulations predict that even if local and direct fingerprints of buried chemical modification are very difficult to image, the delocalization of the doping charges on the neighboring plane of bilayer graphene leads to a clear modification of the symmetry of the STM patterns, dependent on the bias voltage, for both top doped and buried doped layers.

II. METHODOLOGY

Using density functional theory implemented in the SIESTA package,[21] the *N* and *B* doping is investigated in Bernal (*AB*) bilayer graphene. A supercell technique (10×10 unit cell including 399 C atoms and one dopant) was used to investigate doped bilayer graphene, with a vacuum region of $\sim$10 Å in order to avoid undesired interactions between periodically repeated images along the direction perpendicular to the sheets. Exchange-correlation effects were handled within the local density approximation (LDA) as proposed by Perdew and Zunger.[22] Core electrons were replaced by nonlocal norm-conserving pseudopotentials.[23] The valence electrons were described by localized pseudoatomic orbitals with a double ζ.[24] The first Brillouin zone (BZ) was sampled with a $6 \times 6 \times 1$ grid generated according to the Monkhorst-Pack scheme.[25] Real-space integration was performed on a regular grid corresponding to a plane-wave cutoff around 300 Ry. All the atomic structures of self-supported doped bilayer graphene have been relaxed in the plane (with fixed lattice parameters for the supercell) using a conjugate gradient scheme until the maximum residual forces on each atom were smaller than 0.01 eV/Å. The interlayer distance has been kept constant at 3.35 Å, as discussed below.

The STM topological images were calculated according to the Tersoff and Hamann approximation, following the methodology applied for single-layer doped graphene.[16,26] In this approach, applying a small bias voltage (V_{bias}) between the

tip and the sample yields a tunneling current (I) proportional to the local density of states (LDOS) integrated from $E_F - eV_{\text{bias}}$ to E_F:

$$I \sim \int_{E_F - eV_{\text{bias}}}^{E_F} \sum_{i}^{\text{levels}} \sum_{\vec{k}\in \text{BZ}} |\varphi_{i,\vec{k}}(\vec{r})|^2 \delta(E_{i,\vec{k}} - E) dE. \quad (1)$$

Within this framework, a positive (negative) V_{bias} provides information on the electron density corresponding to the occupied (unoccupied) states. In the present work, STM images are calculated in constant current (CC) mode according to standard experimental procedures. The tip-sample distance (or tip height) is defined as the distance between the atomic plane and the pointlike tip, implying that neither the tip shape nor its electronic structure are taken into account in our simulations. Consequently, although the modifications of the tip-sample distance are well described within the present approach, the value of the tip-sample distance cannot be directly compared with the experimental one.

III. ELECTRONIC PROPERTIES OF DOPED BILAYER GRAPHENE

In this work, asymmetric (one of the two layers) substitutional doping of AB stacked BLG is considered. In the substitution process, two possible sites exist, related to the two inequivalent C atoms of pristine BLG. If the substituting dopant is on the top of the center of a hexagon of the neighboring layer, the substitution is defined as type 0 [site 0 substitution—Fig. 1(d)]. On the contrary, if the dopant lies at the top of another carbon atom in the neighboring layer (A-type atom), the substitution is defined as type 1 [or site 1 substitution—Fig. 1(d)]. According to the supercell size described above, the doping concentration is 0.5% on the doped layer or 0.25% of the complete bilayer system.

After full *ab initio* optimized relaxation, no important structural modifications of the graphene layer are observed for type 0 or type 1 and B/N substitutional doping. The bond length between the dopant and the nearest-neighbor C atom is slightly modified but less than for CNT doping.[16] Indeed, the N-C bond is nearly unchanged (small reduction of 0.01 Å) and the B-C bond increases to 1.47 Å compared to 1.42 Å for the C-C bond in pristine graphene. However, no relaxation has been performed regarding the interlayer separation, since DFT is known to not properly describe long-range weak interactions (van der Waals type).[27] Moreover, experimental data of N-doped MLG have not concluded in any change related to the interlayer distance.[11,12] However, we have carefully checked that our theoretical predictions are not dependent on the exact interlayer distance. For example, a reduction of 0.2 Å (a realistic maximal value for the possible variation of the interlayer distance due to the doping) does not change notably the energy band dispersion and modifies slightly (by ∼0.05 eV) the position of the Fermi energy of the doped system.

In Fig. 1, the electronic band structure of pristine bilayer graphene [Fig. 1(a)] is compared with N-doped [Fig. 1(b)] and B-doped [Fig. 1(c)] BLG for the two possible substitutions (types 0 and 1 corresponding to solid and dashed lines, respectively). The well-known quadratic dispersion near the K point and the small overlap between the valence and conduction bands of the pristine bilayer[3] is clearly illustrated in Fig. 1(a). A gap opening is predicted for both N-doped [Fig. 1(b)] and B-doped [Fig. 1(b)] bilayers. This feature is very similar to the effect of an applied external electric field on the electronic levels, as recently studied in Ref. 20. In this work, this gap opening is found to be very similar for both types of substitutional doping [Figs. 1(b) and 1(c)], although with a slightly larger value for type-0 doping due to the more important charge transfer from the doped layer to the neighboring one (see below).

The Kohn-Sham band-gap energy (E_g) is calculated to be 0.21 and 0.13 eV for type-0 and -1 bilayer systems, respectively. These E_g values have to be considered with care since DFT is known to always underestimate the electronic band gap. Although the DFT approach has also been used in Ref. 20 to estimate the band gap in asymmetric doped bilayer graphene, our calculations predict a larger band gap by 0.1 eV for type-0 doping with the same concentration. Such a discrepancy can be explained by the different exchange-correlation functionals

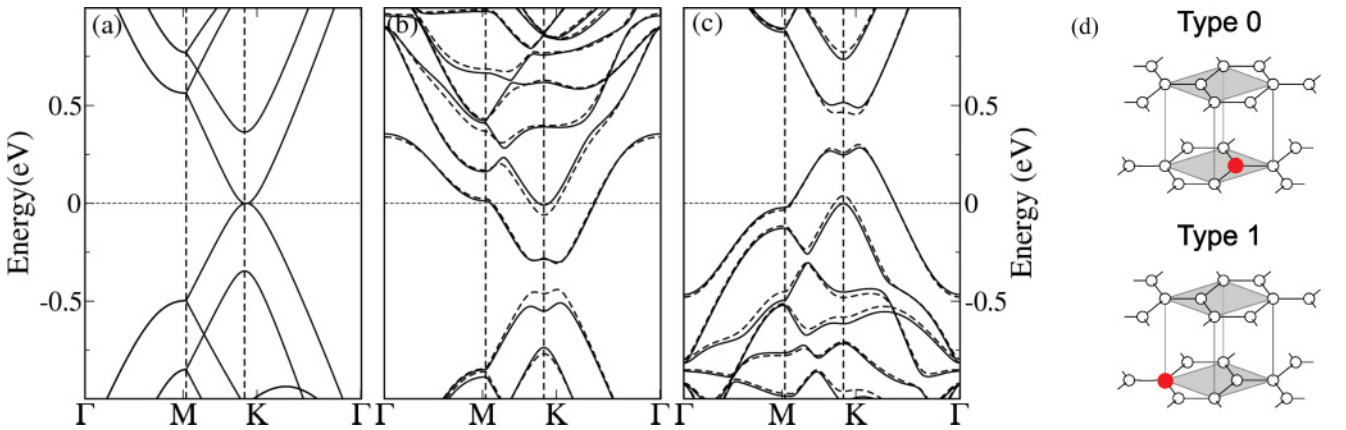

FIG. 1. (Color online) *Ab initio* electronic band structures of (a) pristine, (b) N-doped, and (c) B-doped bilayer graphene. Only one of the two layers is doped by substitution of a single carbon atom. Type 0 (solid line) and type 1 (dashed line) doping sites are considered. A 10 × 10 supercell was used to model the three systems, including 399 C atoms and one dopant. (d) Schematic representations of type 0 (top) and type 1 (bottom) doping. Open (solid) symbols represent the carbon atoms (the dopant).

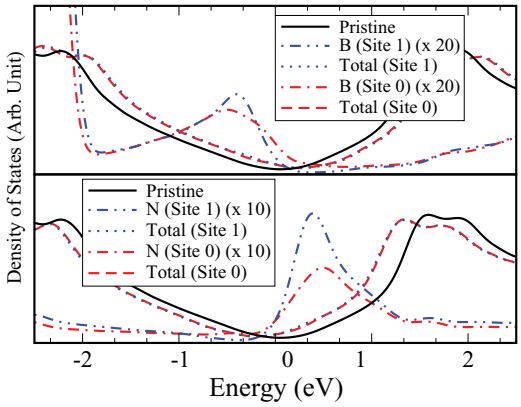

FIG. 2. (Color online) *Ab initio* electronic densities of states (DOS) for (top) B-doped and (bottom) N-doped bilayer graphene. Red dot-dashed lines (blue dotted lines) represent the total DOS for type 0 (type 1). The dot-dashed lines (dot-dot-dashed lines) illustrate the partial densities of states (PDOS) located on the (B or N) dopant site on site 0 (1). The DOS of pristine bilayer graphene is depicted by the black solid line.

used (the generalized gradient approximation in Ref. 20 and the local density approximation in the present work). Finally, the difference between the valence and conduction bands at the point K of the Brillouin zone (named U in Ref. 28) is 0.23 and 0.33 eV, respectively, for type-0 and type-1 doping.

The densities of states (DOS's) of the doped bilayer graphene resulting from first-principles electronic structure calculations are displayed in Fig. 2. The DOS of pristine graphene is given for comparison (black solid line). The doping by a trivalent atom (boron case) leads to an upshift of the Fermi level (E_F) by 0.3 eV, equivalent to a p-type behavior in conventional semiconductor physics. The partial density of states (PDOS) on a B atom exhibits a local electronic state (resonant state) at -0.4 eV in the valence band. In contrast, the N doping induces an excess of electrons (due to the substitution of a C atom by a pentavalent atom), leading to a traditional n-type behavior. Consequently, the E_F is downshifted by 0.3 eV and the corresponding PDOS on the N atom presents a resonant peak at $+0.4$ eV. This chemical doping picture is similar to the ones reported for single-layer graphene[16,29] and carbon nanotubes.[15] However, the shift of the Fermi level is found to be smaller in a bilayer system than for single-layer graphene, due to the partial transfer of extra electrons (or holes) to the neighboring carbon layer (see below). Figure 2 also confirms that type-0 or type-1 doping generates similar electronic properties.

IV. STM IMAGES OF DOPED BILAYER GRAPHENE

In this section, first-principles calculations are performed to simulate STM images of asymmetrically doped bilayer graphene. Although quite scarce, experimental STM investigations of chemical doping in graphene-based material have mainly focused on the monoatomic layer (SLG),[13] or on multilayered systems[12] without real discrepancies with SLG. Theoretical STM images of B- and N-doped SLG have already been published previously,[16] and are very similar (as will be demonstrated later on) to the local patterns of doped BLG when

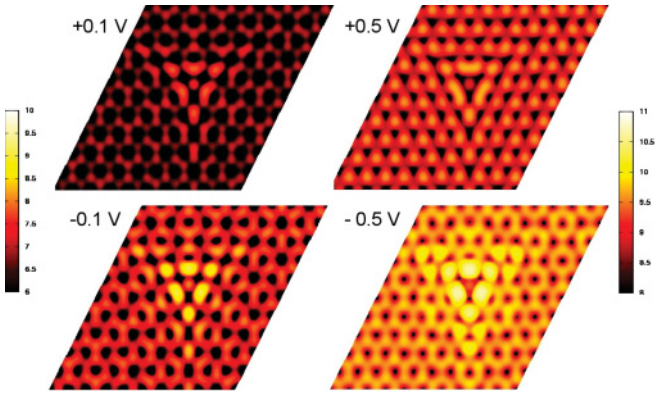

FIG. 3. (Color online) *Ab initio* STM images of N-doped bilayer graphene for various bias voltages: $+0.1$ V (top left), $+0.5$ V (top right), -0.1 V (bottom left), and -0.5 V (bottom right), respectively. The nitrogen dopant is located at the center of the pattern, on the top layer.

the substitution appears on the top surface layer. In contrast, the buried dopant will have a drastic influence on the STM pattern. In the following, the study will focus on type-0 doping since type-1 doping leads to similar conclusions, as expected due to the similar electronic structures described above.

Figures 3 and 4 present the *ab initio* simulations of STM images for bilayer graphene with the dopant located on the top layer. The local signatures are indeed very similar to the STM images obtained for a N or B dopant embedded in single-layer graphene.[13,16] The N substitution induces a triangular pattern centered on a dark region located on the N atom (Fig. 3). This specific signature has been interpreted in terms of the spatial extension of the electronic states associated with the N atom and the three neighboring carbon atoms (forming the three C-N bonds) in the direction perpendicular to the graphene plane.[16] Recent experimental STM measurements have confirmed this symmetry in the local STM pattern of the substituting N dopant.[13] Similarly, the B substitution exhibits a very bright spot centered on the dopant site, related to the large extension of the atomic orbitals centered on the dopant

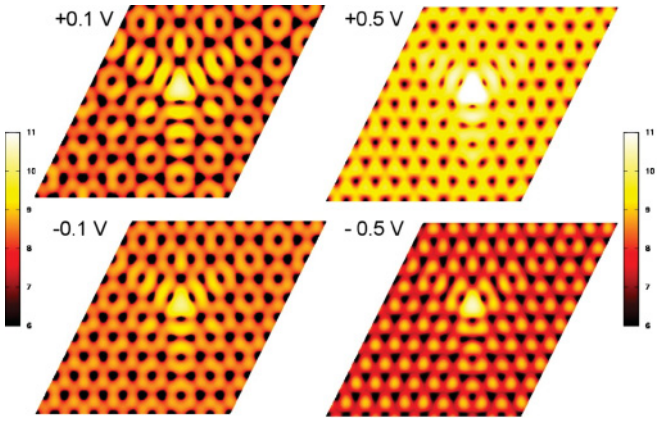

FIG. 4. (Color online) *Ab initio* STM images of B-doped bilayer graphene for various bias voltages: $+0.1$ V (top left), $+0.5$ V (top right), -0.1 V (bottom left), and -0.5 V (bottom right), respectively. The boron dopant is located at the center of the pattern, on the top layer.

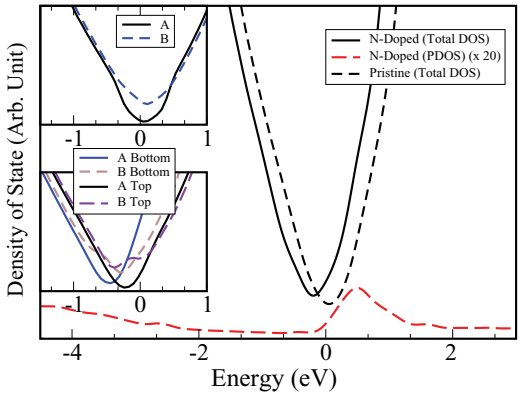

FIG. 5. (Color online) Main panel: DOS for the N-doped graphene bilayer (solid black line) compared with the pristine bilayer graphene (short-dashed line). The long-dashed red curve corresponds to the nitrogen PDOS. Top inset: Respective PDOS for A- and B-type carbon atoms in pristine bilayer graphene. Bottom inset: Respective PDOS for A- and B-type carbon atoms in the N-doped (bottom) and undoped (top) graphene layers. In each panel, the charge-neutrality point (Fermi energy) is located at zero energy.

with an extra electronic charge (Fig. 4). The asymmetry of the local contrast with both the sign and the value of the bias voltage is directly related to the energy of the localized state associated with B doping, which could be an important aspect to interpret the corresponding experimental images.

In STM, the main difference between SLG and AB-stacked pristine BLG is the observed asymmetry at low bias voltage between the carbon atoms from the two different sublattices, which are either A or B type. B-type carbon atoms (lying on the top of the center of a hexagon of the neighboring layer) appear much brighter than A-type carbon atoms (lying on the top of another carbon atom from the neighboring layer), leading to a triangular-lattice pattern frequently observed by STM. This interlayer interaction effect in graphite on the STM pattern has been explained based on a pure electronic density effect.[30,31] Indeed, the *ab initio* DOS of the pristine bilayer obtained by DFT is illustrated in Fig. 5, including a PDOS on A- and B-type carbon atoms (top inset). The A-type carbon atom presents a vanishing PDOS near the Dirac point, while the PDOS of a B-type carbon atom exhibits a plateau between -0.4 and $+0.4$ eV. At a given bias voltage, the STM image is directly related to the local electronic states integrated from E_F to $E_F - eV_{\text{bias}}$. Consequently, for a small bias voltage ($<$0.4 V), only the B-type carbon atoms are visible, whereas a larger bias voltage gives rise to a hexagonal pattern containing all the carbon atoms imaged as bright spots.[32]

However, because of the (almost) symmetrical DOS at E_F, the difference of brightness (or apparent height) of A- and B-type carbon atoms will not be dependent on the sign of the bias voltage. Coming back to Fig. 3, a triangular pattern (of the carbon network) can be clearly observed away from the local fingerprint of the N dopant for a bias voltage of $+0.5$ eV, while a -0.5 V bias voltage displays a hexagonal pattern. In contrast, for the B-doped bilayer graphene (Fig. 4), a triangular pattern can be observed for a bias voltage of -0.5 V, while A- and B-type carbon atoms have a similar brightness at $+0.5$ V.

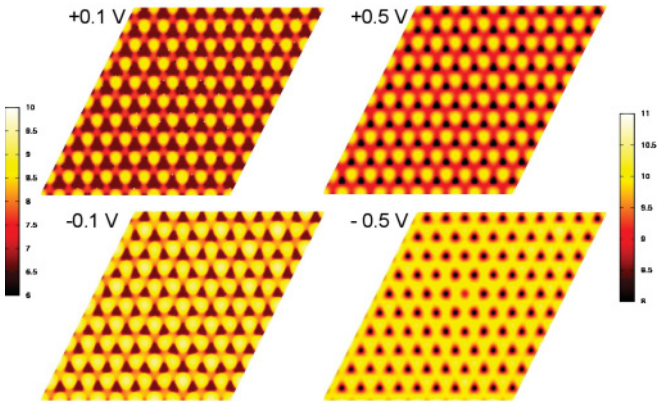

FIG. 6. (Color online) *Ab initio* STM images of N-doped bilayer graphene for various bias voltages: $+0.1$ V (top left), $+0.5$ V (top right), -0.1 V (bottom left), and -0.5 V (bottom right), respectively. The nitrogen atom is located at the center of the pattern, in the neighboring underlayer (buried dopant).

Ab initio STM images of buried N and B in bilayer graphene are represented in Figs. 6 and 7, respectively. The first observation is the absence of a local signature in the (perfect) layer, which is on top of the doped layer containing the buried dopant (at the center of the image). Note that a faint local pattern could appear in our simulations at high bias voltage, but it will certainly be difficult to observe such a tiny modification of the contrast experimentally. Consequently, as expected for MLG, the local electronic states of the buried dopant in the neighboring underlayer are totally screened by the first pristine layer.

In the following, the contrast between the A- and B-type carbon atoms is analyzed in N-doped (Fig. 6) and B-doped (Fig. 7) bilayer graphene. In both cases, a triangular-symmetry pattern can be observed in Figs. 6 and 7 for small bias voltages ($\pm$0.1 eV), although the contrast is found to be dependent on the sign of the bias voltage. However, for higher bias voltage, STM images exhibit a hexagonal symmetry pattern (all carbon atoms identical) for $V_{\text{bias}} = -0.5$ eV in N-doped bilayer and for $V_{\text{bias}} = +0.5$ eV in B-doped bilayer. In contrast,

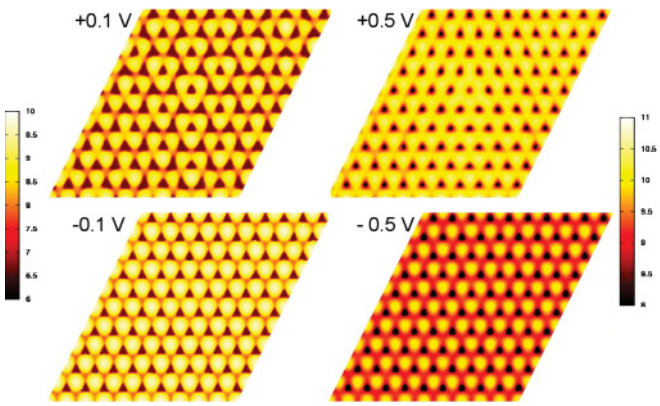

FIG. 7. (Color online) *Ab initio* STM images of B-doped bilayer graphene for various bias voltages: $+0.1$ V (top left), $+0.5$ V (top right), -0.1 V (bottom left), and -0.5 V (bottom right), respectively. The boron atom is located at the center of the pattern, in the neighboring underlayer (buried dopant).

the triangular-symmetry pattern (where only B-type carbon atoms are visible) is conserved for the opposite sign of the bias voltage: $V_{\text{bias}} = +0.5$ V in N-doped bilayer and $V_{\text{bias}} = -0.5$ V in B-doped bilayer.

In order to scrutinize and analyze more deeply these STM contrast differences, a close-up view of the DOS of pristine and N-doped bilayer graphene is presented in Fig. 5. Due to N doping (donor character), the Fermi energy is found to be 0.3 eV above the conventional Dirac point, leading to a DOS asymmetry around the charge-neutrality point (E_F). This downshift of the Dirac point compared to the pristine case is the first step toward explaining the constant differences observed in the STM images when applying various bias voltages.

The second step consists in decomposing the total DOS into PDOS located on the nitrogen atom (Fig. 5). The PDOS located on both A- and B-type carbon atoms are also displayed in the two sheets (the dopant being in the bottom layer) of the N-doped bilayer system (bottom inset), and are compared to the A- and B-type carbon atoms of pristine bilayer graphene, as already mentioned above. Figure 5 (bottom inset) clearly demonstrates that A- and B-type carbon atoms can be differentiated in both pristine and doped layers. In addition, the upshift of the Fermi energy related to the Dirac point is directly connected to the charge transfer from the N dopant to the graphene network. Consequently, the corresponding downshift of the Dirac points in both layers clearly suggests that electronic charge transfer occurs in the two sheets, although only the bottom layer is intrinsically doped. Nevertheless, the downshift of the Dirac point is obviously found to be larger for the layer hosting the dopant (bottom layer) than the other one (top layer). Indeed, densities of charge carrier have been computed by integrating the DOS from its minimal value (Dirac point) to the Fermi level: $n_{\text{top}} = 0.75 \times 10^{13}$ and $n_{\text{bottom}} = 2.06 \times 10^{13}$ electrons per cm^2 are estimated for the top and the bottom layers, respectively, which correspond to 0.19 and 0.52 electron per N atom.

This charge difference ($\Delta_n = n_{\text{bottom}} - n_{\text{top}}$) between the two layers results in different local electrostatic potentials on each layer. Consequently, a gap opening is induced in the doped BLG (Fig. 1) in the same way as when an external electric field is applied to the system.[8,9] Indeed, the electric field of a planar capacitor with the same charge density would be $V = 118$ mV/Å. The ratio $\alpha = U/(\Delta_n)$ (where U is the energy gap at the K point, as defined before) gives the linear relation between the charge-density difference and the value of the resulting band gap. Here, we obtain a value of 14.2×10^{12} cm^2 meV, a number comparable to the value suggested in Ref. 28 for an external applied electric field. In conclusion, the present analysis reinforces the interpretation of the gap opening in asymmetric doping in terms of the electrostatic potential difference, related to the charge transfer between layers.

Coming back to the STM images, the contrast difference between the A- and B-type carbon atoms in N-doped bilayer graphene can be easily interpreted in terms of the local density of states around the Fermi level. In fact, probing the electronic states in the energy window $[E_F;\ E_F + 0.5$ eV] for N-doped bilayer induces a similar contrast for both A- and B-type carbon atoms, thus explaining the hexagonal-symmetry pattern in Figs. 3 and 6 (bottom right). However, if the bias voltage is positive, the energy window $[E_F;\ E_F - 0.5$ eV] has to be considered, leading A-type carbon atoms to contribute less to the STM images as depicted in the PDOS. Hence, the corresponding STM images present a triangular network formed by the B-type carbon atoms, as illustrated in Figs. 3 and 6 (top right). In contrast, for a lower negative bias ($V = -0.1$ eV), the bottom layer presents a larger contrast than the top layer [Figs. 3 and 6 (top left)] due to the small energy density on A-type carbon atoms in the energy window $[E_F;\ E_F - 0.1$eV] [see Fig. 5 (bottom inset)]. Finally, an analogous analysis can be performed for the B-doped system. Indeed, with the acceptor character of the dopant, the Fermi energy appears below the Dirac point, leading to similar effects (although inverses with the sign of the bias voltage) on the STM contrast difference between the A- and B-type carbon atoms in B-doped bilayer graphene (see Figs. 4 and 7).

V. CONCLUSION

In conclusion, *ab initio* electronic structure calculations and STM images (within the Tersoff-Hamann approach) have been investigated in asymmetric nitrogen and boron substitution in bilayer graphene. Our first-principles calculations reveal that both the electronic structure and the STM images are independent of the position of the dopant (site 0 or site 1 for the substituting dopant). The local STM signatures of the dopant are very similar to the one observed for doped monolayer compounds. Our simulations also predicted that buried N and B dopant (in the bottom layer) substitution does not lead to a specific local fingerprint on the top layer. The symmetry of the predicted STM patterns in bilayer graphene can be either hexagonal (when all carbon atoms are imaged) or triangular (when only B-type carbon atoms are imaged). This situation is modified when introducing dopants in the top layer or incorporating buried dopant in the bottom layer. In addition, the dopant localization (either on the top or bottom layer) has been found to drastically influence at which bias voltage value the hexagonal symmetry will be recovered. This theoretical prediction has been accurately investigated and is supported by a detailed PDOS analysis of A- and B-type carbon atoms in both pristine and doped bilayer systems. Of course, this phenomenon will strongly depend on the amount of doping (amount of charge transfer) on the top layer of a multilayer AB-stacked graphene, but could also appear when applying an external field or resulting from the interaction with a substrate. The relative orientations of the layers are also an important consideration. Indeed, misoriented multilayer graphene will not, in general, give rise to such asymmetry in the STM contrasts, since all carbon atoms have a similar environment and cannot really be distinguished as A or B type in these systems.[4,5] These theoretical predictions could be verified experimentally by measuring a series of STM images at various bias in N- or B-doped bilayer graphene. The shift of the Fermi level (related to the Dirac point) and the opening of a band gap without gating could also be investigated by STS techniques. In the present work, only bilayer graphene systems have been investigated. For multilayer graphene (with a larger number of layers), analogous effects are expected to be observed. However, the amount of charge transfer to the top layer in the case of a deeply buried defect could be modified

by a third layer or by the presence of a substrate. In any case, the theoretical predictions proposed in the present work are expected to stimulate experimental STM images in doped Bernal-stacked multilayer graphene.

ACKNOWLEDGMENTS

L.H. thanks Sylvain Latil for his help with the drawing of Fig. 1(d). This work is directly connected to the BNC-TUBE STREP EU project (Project No. 033350), to the Belgian Program on Interuniversity Attraction Poles (PAI6) on "Quantum Effects in Clusters and Nanowires," and to the ARC on "Graphene StressTronics" (Convention No. 11/16-037) sponsored by the Communauté Française de Belgique, and to the European Union through the ETSF e-I3 project (Grant No. 211956). Computational resources were provided by the Interuniversity Scientific Computing Facility located at the University of Namur, Belgium, which is supported by the F.R.S.-FNRS under convention No. 2.4617.07. S.O.G. acknowledges financial support from the FRIA.

*Department of Materials Science and Engineering, University of Wisconsin-Madison, Madison, WI 53706-1595, USA.

[1]K. S. Kim *et al.*, Nature (London) **457**, 706 (2009).
[2]F. Schwiertz, Nat. Nanotech. **5**, 487 (2010).
[3]S. Latil and L. Henrard, Phys. Rev. Lett. **97**, 036803 (2006).
[4]S. Latil, V. Meunier, and L. Henrard, Phys. Rev. B **76**, 201402 (2007).
[5]F. Varchon, P. Mallet, L. Magaud, and J. Y. Veuillen, Phys. Rev. B **77**, 165415 (2008).
[6]G. T. DeLaissardière, D. Mayau, and L. Magaud, Nano Lett. **10**, 804 (2010).
[7]K. S. Novoselov *et al.*, Nat. Phys. **2**, 177 (2006).
[8]J. B. Oostinga *et al.*, Nat. Mater. **7**, 151 (2008).
[9]M. Aoki and H. Amawashi, Solid State Commun. **142**, 123 (2007).
[10]B. Guo *et al.*, Nano Lett. **10**, 4975 (2010).
[11]D. Wei *et al.*, Nano Lett. **9**, 1752 (2009).
[12]D. Deng *et al.*, Chem. Mater. **23**, 1188 (2011).
[13]L. Zhao *et al.*, Science **333**, 999 (2011).
[14]X. Wang *et al.*, Science **324**, 768 (2009).
[15]S. Latil, S. Roche, D. Mayou, and J.-C. Charlier, Phys. Rev. Lett. **92**, 256805 (2004).
[16]B. Zheng, P. Hermet, and L. Henrard, ACS Nano **4**, 4165 (2010).
[17]Y. Wang *et al.*, ACS Nano **4**, 1790 (2010).
[18]Y. J. Cho *et al.*, J. Phys. Chem. C **115**, 9451 (2011).
[19]H. M. Jeong *et al.*, Nano Lett. **11**, 2472 (2011).
[20]M. G. Menezes, R. B. Capaz, and J. L. B. Faria, Phys. Rev. B **82**, 245414 (2010).
[21]D. Sánchez-Portal, P. Ordejón, E. Artacho, and J. M. Soler, Int. J. Quantum Chem. **65**, 453 (1997).
[22]J. P. Perdew and A. Zunger, Phys. Rev. B **23**, 5048 (1981).
[23]N. Troullier and J. L. Martins, Phys. Rev. B **43**, 1993 (1991).
[24]E. Artacho *et al.*, Phys. Status Solidi B **215**, 809 (1999).
[25]H. J. Monkhorst and J. D. Pack, Phys. Rev. B **13**, 5188 (1976).
[26]J. Tersoff and D. R. Hamann, Phys. Rev. Lett. **50**, 1998 (1983).
[27]New hybrid functionals have been recently developed to overcome this limitation but have not been used in the present study. For example, see K. K. Lee, E. D. Murray, L. Kong, B. I. Lundqvist, and D. C. Langreth, Phys. Rev. B **82**, 081101 (2010).
[28]P. Gava, M. Lazzeri, A. M. Saitta, and F. Mauri, Phys. Rev. B **79**, 165431 (2009).
[29]A. Lherbier, X. Blase, Y. M. Niquet, F. Triozon, and S. Roche, Phys. Rev. Lett. **101**, 036808 (2008).
[30]D. Tománek and S. G. Louie, Phys. Rev. B **37**, 8327 (1988).
[31]J.-C. Charlier, J.-P. Michenaud, and P. Lambin, Phys. Rev. B **46**, 4540 (1992).
[32]P. Lambin, H. Amara, J.-C. Charlier, and V. Meunier, in *Chemistry of Carbon Nanotubes*, edited by V. Basiuk and E. Basiuk (American Scientific Publishers, Stevenson Ranch, USA, 2008), Vol. 3, pp. 75–83.